www.amlett.com, www.amlett.org, DOI: 10.5185/amlett.2013.8529 Published online by the VBRI press in 2013

Structural, optical and magnetic properties of (Fe, Ag) co-doped ZnO nanostructures

B. Sankara Reddy[1], S. Venkatramana Reddy[1*], N. Koteeswara Reddy[2], Y. Prabhakara Reddy[3]

[1]*Department of Physics, Sri Venkateswara University, Tirupati 517 502, Andhra Pradesh, India*
[2]*Center for Nanosciaence and Engineering (CeNSE), Indian Institute of Science, Bangalore 560012, India*
[3]*Department of Physics, Sri Padmavati Mahila Visvavidyalayam, Tirupati 517502, A.P., India*

[*]Corresponding author. Tel: (+91) 8772289472; Fax: (+91) 8772248485; E-mail: drsvreddy123@gmail.com

Received: 08 August 2013, Revised: 29 September 2013 and Accepted: 18 October 2013

ABSTRACT

The (Fe, Ag) co-doped ZnO nanostructures are developed through chemical precipitation method at various percentages of Fe. The X-ray diffraction studies suggest that all the as-synthesized (Fe, Ag) doped ZnO nanopowders have single phase wurtzite structure with no secondary phases. However, the positions of diffracted peaks slightly shifted towards lower (2θ) angles. Photoluminescence studies reveal that 1 mol% of Fe doped ZnO sample has the best ultra violet (UV) emission properties than the other samples. On the other hand, 5 mol% of Fe doped ZnO nanopowders consists of strong green emission band, which belongs to oxygen interstitial defect states. Magnetization analysis shows that 5 mol% of Fe doped ZnO nanopowders have highest room temperature ferromagnetism (RTFM) than the RTFM of other samples. The observed RTFM in co-doped ZnO nanopowders is discussed with the help of structural and emission studies. The results strongly suggest the future development of efficient luminescence and magnetic materials at normal laboratory temperatures with (Fe, Ag) co-doped ZnO nanostructures.

Keywords: Co-doped ZnO; nanoplates; HRTEM; optical properties; ferromagnetism.

B. Sankara Reddy is presently a Ph.D student in the Department of Physics, Sri Venkateswara University, Tirupati, Andhra Pradesh, India. He obtained his M.Sc. degree in Physics from Acharya Nagarjuna University, Guntur, India. He is doing research on synthesis and characterization of transition metal doped ZnO nanostructured materials based dilute magnetic semiconductors due to their potential applications in optoelectronics and spintronics devices.

S. Venkatramana Reddy received M.Phil. and Ph.D. degrees in Physics in 1996 and 2001 respectively from Sri Venkateswara University, Tirupati, India. He is Fellow, Institution of Electronics and Telecommunication Engineers, New Delhi, and Life member in many Professional Bodies like the Instrument Society of India, Bangalore, Semiconductor Society, India, New Delhi, Indian Physics Association, BARC, Mumbai, Indian Association of Physics Teachers, Kanpur, Uttar Pradesh, Senior Member in International Association of Computer Science and Information Technology, Member in International Association of Engineers. He is doing research in the area of nanomaterials and electronics. Presently he is working as an Assistant Professor.

N. Koteeswara Reddy obtained M.Sc. and Ph.D. degrees from Sri Venkateswara University, Tirupati. He is working on the synthesis of various thin films and nanostructured materials. He worked as a Postdoctoral fellow with various international groups including Prof. Y. B. Hahn, Prof. F. Patolsky, and Prof. C. W. Tu. Recently he joined as Postdoc in Humboldt University, Berlin, Germany under the Marie Curie International Incoming Fellowship 2012 with Prof. Nicola Pinna group. Dr. Reddy had nearly 65 research articles in international pre reviewed journals.

Introduction

Zinc oxide (ZnO) is a II-VI group semiconductor and has direct band gap energy of 3.37 eV and large exciton biding energy of 60 meV at room temperature. ZnO has attracted the attention of researchers from several decades due to its many important technological applications such as optics, optoelectronics, magneto electronics, highly efficient blue LEDs and microwave devices **[1-5]**. On the other hand, nanostructured ZnO acts as a dilute magnetic semiconductor (DMS) and has focused great attention for the design of many devices by manipulating the spin based electronics (spintronics) [**1**]. The recent available reports on ZnO doped with transition metal (TM) ions, indicate a number of applications including room temperature (RT) nanolasers, n-type doping, p-type doping and RT ferromagnetic semiconductor nanomaterials **[6-10].** Dietl et al. **[11]** and Sato et al. **[12]** have predicted the room

temperature ferromagnetism (RTFM) in transition metal doped ZnO, and further, there has been a lot of research work carried on ZnO based dilute magnetic semiconductors (DMS). Many researchers have been described the presence of ferromagnetism in transition metal (Co, Mn, Fe, Ni, Cr, etc) doped ZnO using the defects related mechanism, hole mediated exchange interactions, secondary phases, bound magnetic polorans (BMPs), clusters, organic capping agents, synthesis methods etc. at lower and high Curie temperatures **[13-18].** However, a few other research groups have reported the absence of ferromagnetism in ZnO, even when doped with transition elements of the same kind **[19-21].** Further, some research groups have investigated ferromagnetism in ZnO without doping of transition metal impurities **[22].** A few other research groups studied the magnetic properties of multiple ions doped (or) co-doped ZnO nanomaterials **[23, 24].** However, the real origin of ferromagnetism is still controversial. From our earlier studies it is noticed that silver (Ag) acts as an excellent neutralizer of native defect states in ZnO and enhances the optical properties **[25]**. In this direction, trails have been made to minimize the native defect states by doping with Ag and then doping Fe as a co-dopant into ZnO. This approach allows the researchers to overcome the existing obstacles like formation of alloys, cluster formation, dissolving limitation etc. **[18].**

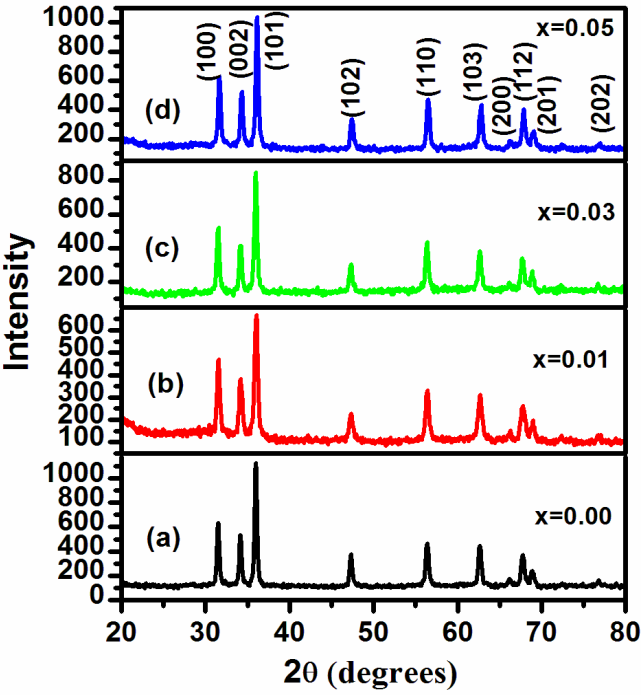

Fig. 1. XRD pattern of (a) undoped ZnO (b) 1 mol% (c) 3 mol% (d) 5 mol% of Fe doped ZnO Nanostructures. (keeping Ag = 5 mol% as constant).

Various types of nano structured materials are synthesized by using different physical methods such as simple vapor transport and condensation process **[3]**, sol-gel method **[26]**, solid state reaction method **[27]**, radio-frequency (rf) magnetron sputtering technique **[28]**, facile low temperature synthesis **[29]**, chemical co-precipitation method **[25]**, etc. Among these methods, chemical co-precipitation method is the best one, because it is simple, inexpensive and high yield rate. In the present work, the $Zn_{1-(x+y)}Fe_xAg_yO$ samples (x = 0.00, 0.01, 0.03 and 0.05; y= 0.00 and 0.05) have been synthesized using chemical co-precipitation method and their composition, structural, optical, and magnetic properties have been investigated.

Experimental

Synthesis of nanostructured materials

For the synthesis of (Fe, Ag) doped ZnO nanopowders, analytical grade zinc acetate dihydrate ($Zn(CH_3COO)_2 2H_2O$), (Merck, 99.8 %, India), potassium hydroxide (KOH) (Merck, 99.9 %, India), ferrous chloride tetra hydrate $FeCl_2{\cdot}4H_2O$ (Merck, 99.8 %, India) and silver nitrate ($AgNO_3$) (Merck, 99.9%, India) have been used. Doped ZnO nanostructures are synthesized at room temperature by following the procedure described elsewhere **[25]**. In brief, 0.2 M equimolar solution is prepared by using precursor materials zinc acetate and KOH. Then ferrous chloride tetra hydrate was added drop-wise with different concentrations varying from 0 to 5 mol% keeping silver nitrate concentration as constant at 5 mol % under continuous stirring for 10 hr. After filtering, the precipitate is washed repeatedly with double distilled water to remove unreacted chemical species. Finally, the product is dried at 70 ºC for 9 hr, and then grounded and annealed in the furnace at 500 °C for 1 hr.

Characterization

The structural properties of the samples are determined by Seifert 3003 TT X-ray diffractometer (XRD) using Cu K_α radiation by applying voltage and current of 40 kV and 30 mA respectively. These properties are confirmed by Transmission Electron Microscopy (TEM) and high resolution TEM (HR-TEM) (Model: JEOL JEM 2100). Surface morphology of the samples is studied by field emission scanning electron microscopy (FE-SEM) (Model: ZEISS ULTRA 55, Gemini) and their elemental composition is estimated by energy dispersive X-ray spectroscopy (EDS) attached with FESEM. Crystallinity of the nano structures are analyzed by micro Raman spectroscopy {Lab RAM HR (Horiba JOBIN-YVON spectrophotometer)}. Photoluminescence (PL) studies are carried out by PL spectrometer (Model: HORIBA Jobin Yvon FluoroLog 3) with a 450 W Xenon arc lamp as an excitation source. Superconducting quantum interference device (SQUID) magnetometer (Quantum Design MPMS - XL) is used to investigate the magnetic properties of the (Fe, Ag) doped ZnO nano powders.

Results and discussion

Structural analysis

The XRD patterns of undoped and (Fe, Ag) co-doped ZnO nanostructures annealed at 500 °C (for 1 hr) are shown in **Fig. 1.** The X-ray diffraction patterns of the all samples are indexed and are found to be matching with the standard hexagonal wurtzite structure of ZnO corresponding to the data card no: JCPDS 36-1451. It reveals that the co-substitution of Fe and Ag does not disturb the wurtzite crystal structure of parent ZnO. Contrary to earlier reports **[30, 31]**, this may be attributed to the limitation of XRD

characterization that small amount of impurities cannot be detected.

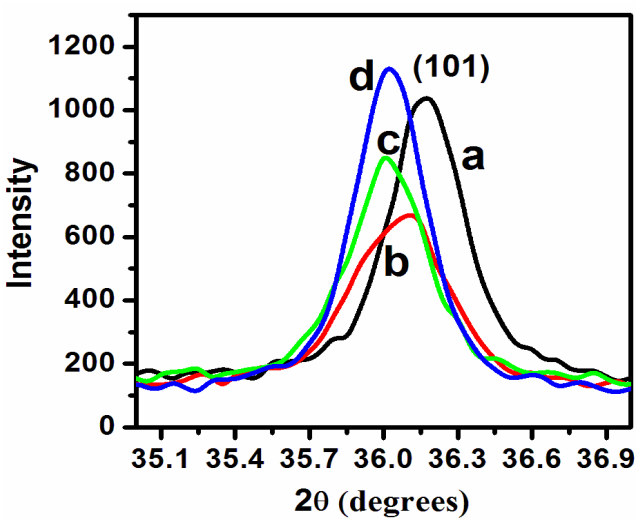

Fig. 2. XRD peak (101) of $Zn_{1-(x+y)}Fe_xAg_yO$ samples shifts towards lower 2θ values.

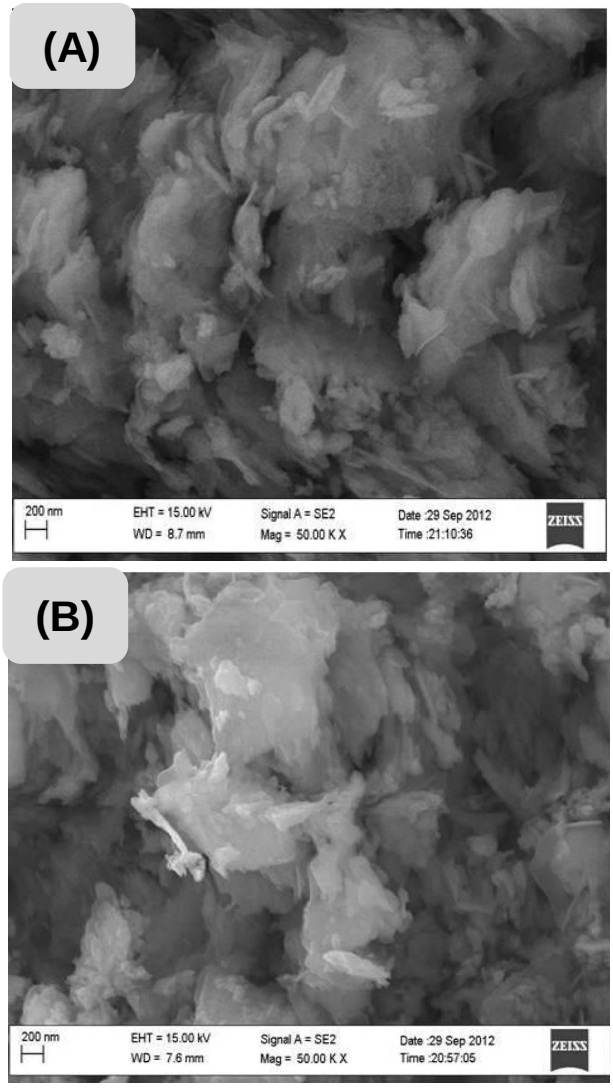

Fig. 3. FE-SEM images of (A) pristine ZnO and (B) $Zn_{0.90}Fe_{0.05}Ag_{0.05}O$ nanostructures.

However, a careful analysis of the peak (101) positions suggests a small shift toward lower 2θ values with increasing Fe doping as shown in **Fig. 2**. The significant change in position of peaks is attributed to the different ionic radii of Zinc, Iron and silver (Zn^{2+} ~ 0.74 Å, Fe^{2+} ~ 0.77 Å and Ag^{+} ~ 0.115 Å). The shifting of the XRD peaks with the co-doped ZnO suggests the substitution of Zn^{2+} by Fe^{2+} in the ZnO host lattice. The similar shift has been reported in transition metal doped ZnO nanostructures by Ekambaram et al**. [32]** and Dinesha et al. **[33].** The size of the particle is very small in the nano scales, which could be the reason for the broadening of XRD peaks. By using Debye-Scheerer formula and the peak (101) of ZnO, the evaluated average particle crystalline size of pristine ZnO, $Zn_{0.94}Fe_{0.01}Ag_{0.05}O$, $Zn_{0.92}Fe_{0.03}Ag_{0.05}O$ and $Zn_{0.90}Fe_{0.05}Ag_{0.05}O$ nanopowders are ~ 23, 19, 21 and 22 nm respectively.

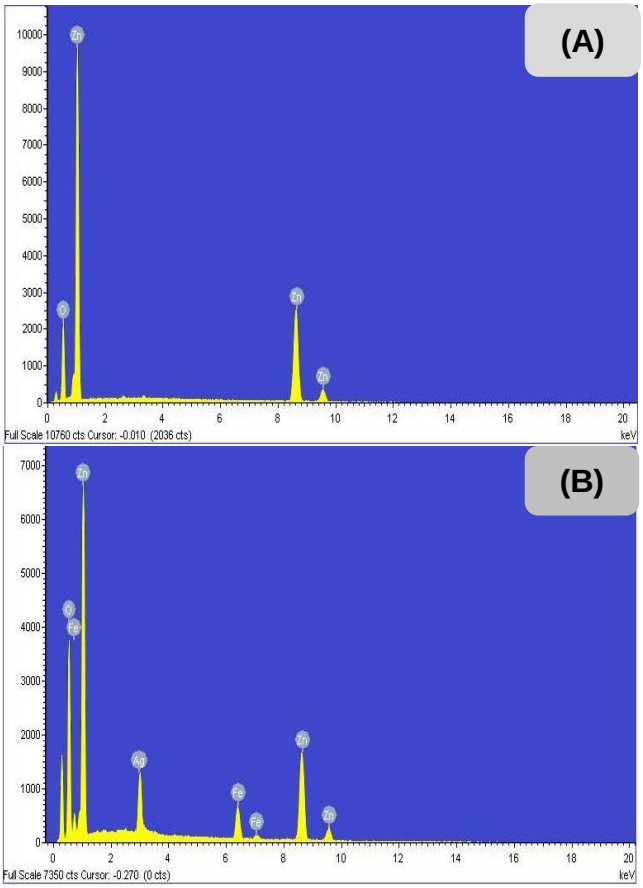

Fig. 4. EDS spectra of (A) pure ZnO and (B) $Zn_{0.90}Fe_{0.05}Ag_{0.05}O$ nanostructures.

Morphological and compositional analysis

FE-SEM micrographs of pristine and 5 mol% of co-doped (Fe, Ag) ZnO nanostructures are shown in **Fig. 3** (A) and (B) respectively. It shows that the pristine ZnO and co-doped ZnO samples consist of meager formation of nanoplates having the diameter of about 200 nm. In particular, there is no appreciable change in the nanostructure morphology of ZnO, when it is doped with 5 mol% of Fe content in addition to silver at 5 mol%. From **Fig. 4**, spectral analysis of typical EDS spectra indicate that the existence of Fe and Ag elements in ZnO lattice, and

pristine ZnO consists of Zn and O elements only, which are in near chemical stoichiometry.

The Fe concentrations in the above mentioned samples are found to be ~ 0.63%, ~ 1.52 % and ~ 2.70 % along with Ag concentration of ~ 0.68%. **Fig. 5** shows the TEM micrographs of pristine ZnO and $Zn_{0.90}Fe_{0.05}Ag_{0.05}O$ nanostructures of sizes are 100 and 50 nm respectively. The nanoplate is almost transparent under the electron beam, indicating that the plate is very thin and the morphology of these nanoplates of nano materials obviously indexed in **Fig. 5 (B).**

The selected area electron diffraction (SAED) pattern has revealed that the nanosheets are of single crystal structure. The high resolution transmission electron microscopy (HRTEM) images of ZnO and $Zn_{0.90}Fe_{0.05}Ag_{0.05}O$ nano structures are shown in **Fig. 6.** The distance between adjacent lattice fringes of (101) planes from the HRTEM image for $Zn_{0.90}Fe_{0.05}Ag_{0.05}O$ nanoplate of about 0.25 nm, which is smaller than that of pristine ZnO of about 0.27 nm. Further, these (HRTEM) image show that the probably substitution of Fe and Ag ions for Zn, in ZnO lattice, is in good agreement with the results of XRD.

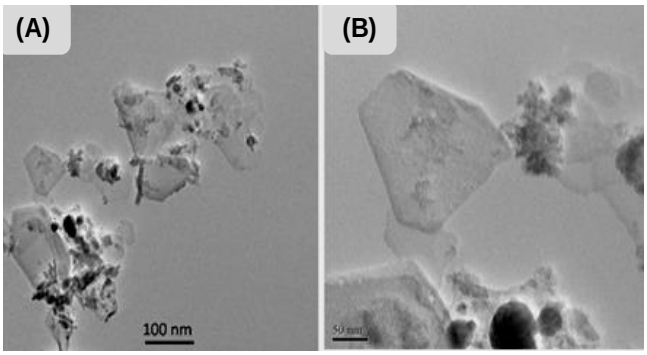

Fig. 5. TEM micrographs of (A) pristine ZnO and (B) $Zn_{0.90}Fe_{0.05}Ag_{0.05}O$ nanostructures.

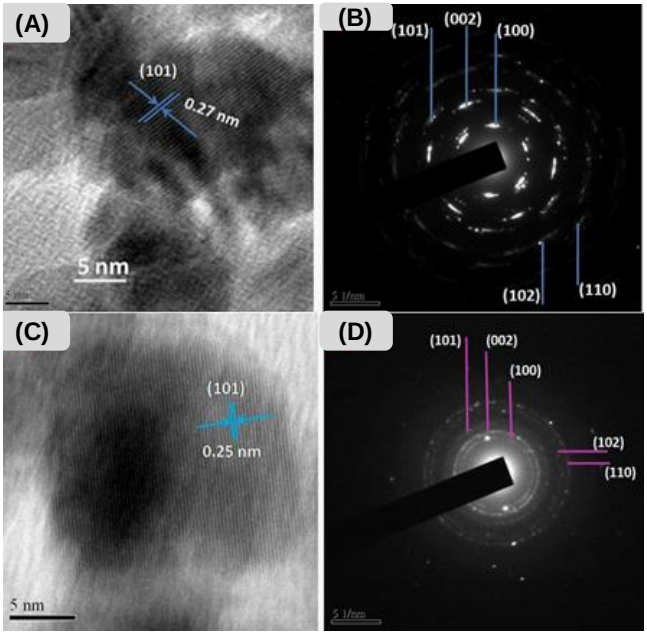

Fig. 6. HRTEM image of (A) pure ZnO and (B) its corresponding SAED pattern, (C) $Zn_{0.90}Fe_{0.05}Ag_{0.05}O$ nano structures and (D) its corresponding SAED pattern.

Raman analysis

Fig. 7 presents the room temperature Raman spectrum of the pristine and co-doped ZnO nanostructures in the range of 50-1200 cm^{-1}. From **Fig. 7 (b-d),** the Raman spectrum of co-doped ZnO shows appreciable changes and can be observed in comparison with the spectrum of undoped ZnO **(Fig. 7 (a)).** The Raman spectrum consists of four peaks located at about 98.65, 380, 435, and 577 cm^{-1}, which correspond to the E_{2L}, A_1 (TO), E_{2H} and A_1 (LO) fundamental phonon modes of hexagonal ZnO respectively. The peak at ~ 330 cm^{-1} is attributed to the multi phonon Raman mode corresponding to the E_{2H}-E_{2L} **[34].** Second order vibrations can be observed in between the band 1030 - 1190 cm^{-1}.

Raman spectra of the co-doped ZnO nanostructures with different Fe concentrations are shown in **Fig. 7 (b-d).** The lower frequency (E_{2L}), higher frequency (E_{2H}) of non polar modes and second order vibration mode have slightly shifted from ~ 98.65 to 97.14 cm^{-1}, ~ 435 to 431 cm^{-1} and ~ 330 to 317 cm^{-1} respectively. The shift of weak band from 380 to 377 cm^{-1} is not marked in **Fig. 7**. All these bands involve only oxygen atoms for all samples **[29]**. The clear blue shifting of these peaks is shown in **Fig. 8**, which indicates the hexagonal wurtzite structure of $Zn_{1-(x+y)}Fe_xAg_yO$ and is in good agreement with the HRTEM and XRD observations. From **Fig. 8**, it is observed that the intensity of the lower frequency peak E_{2L} and the higher frequency peak E_{2H} decrease with the increasing iron dopant concentration. On incorporating Fe into ZnO, the fundamental phonon mode A_1 (LO) is obviously broadened and shifted about 8 cm^{-1} towards lower energy.

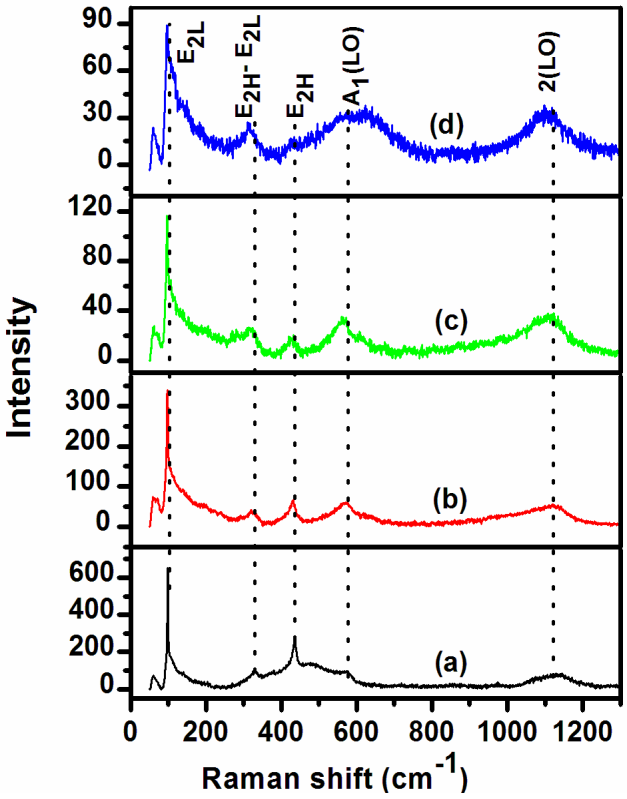

Fig. 7. Raman spectra of (a) pure ZnO (b) 1 mol% (c) 3 mol% (d) 5 mol% of Fe doped ZnO nanostructures.

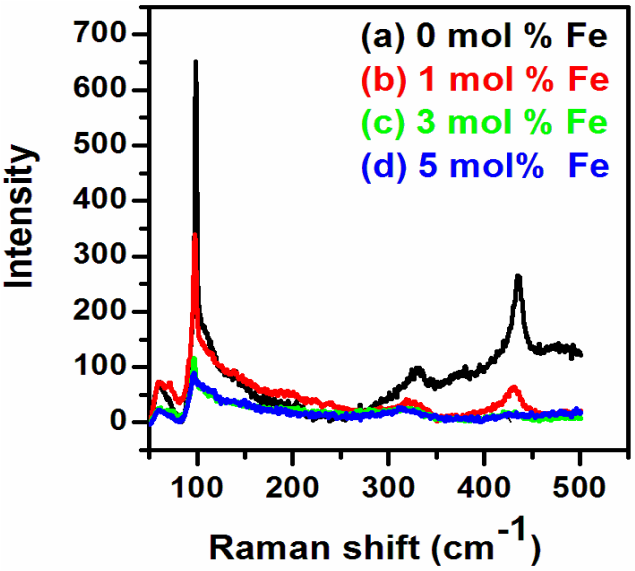

Fig. 8. A clear blue shifting of the Raman peaks in $Zn_{1-(x+y)}Fe_xAg_yO$ nanostructures.

As reported in literature **[35],** such a shift and broadening in the A_1 (LO) phonon mode can be attributed to the scattering contributions of the A_1 (LO) branch outside the brillouin zone center. Zinc interstitials, oxygen vacancies and their defect complexes are mainly responsible for the A_1 (LO) phonon mode **[36, 37].** This reveals that more defects are introduced in these samples and are due to the dopant Fe ions into the ZnO lattice. Raman peak corresponding to the high-energy range observed between ~ 1030 and ~ 1190 cm^{-1} is assigned to the 2(LO) second order polar mode **[38].** The emission is attributed to the deep iron acceptor and intrinsic point defects such as oxygen vacancies, which is evident from Raman and PL results. These Raman studies and the XRD results are in tune with each other.

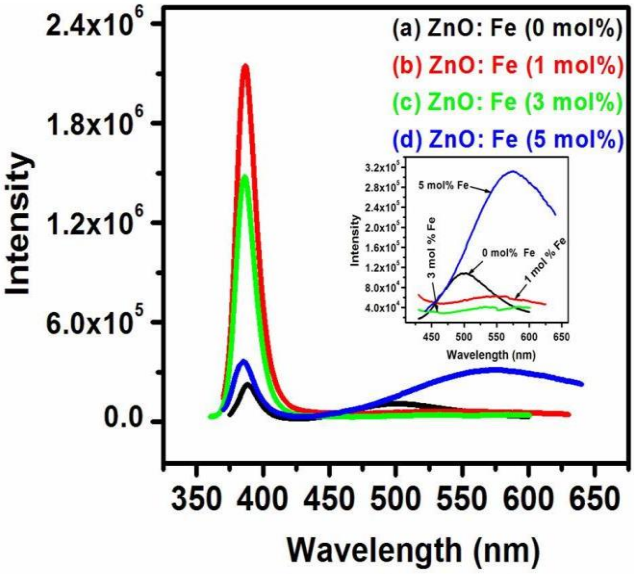

Fig. 9. PL spectra of (a) pure ZnO (b) 1 mol% (c) 3 mol% (d) 5 mol% of Fe doped ZnO nanostructures.

Optical analysis

Fig. 9 shows the room temperature photoluminescence spectra of pristine and co-doped (Fe, Ag) ZnO nanostructures with three doping concentrations. The PL spectrum exhibits two bands, one narrow emission band in UV region and another relatively broad emission band in visible region, under high excitation energy ~ 3.65eV. In the UV spectral range, the intense narrow emission band has appeared in the range ~ 388 (3.19 eV) to ~ 385 (3.22 eV) nm. In general, the UV emission band is the characteristic emission of ZnO and it is attributed to the free excitonic recombination or zinc vacancy related defects in ZnO **[30, 31, 39]**. On increasing the iron doping concentration in ZnO, there is a small change (i.e. slightly shifted towards lower wave length side) in position of the UV emission band. This is presumed to be due to decrease of the size of ZnO nanoplates (as shown in **Fig. 5**). The PL intensity is high for co-doped ZnO nanoparticles as compared to those of undoped ZnO **[28].** But, the undoped ZnO has another defect related broad emission peak in the visible region around 500 nm, which is associated with Zn interstitial defect states.

Contrary to the earlier reports **[15, 40],** for 1 mol% of Fe (at Ag= 5 mol %), the contribution of the intensity of near band edge emission (NBE) peak increases drastically. Further with the increase of the iron content (> 1 mol % up to 5 mol %), the intensity of NBE band emission begins to decrease as suggested by Limaye et al. **[15]**. The quenching of the UV emission is presumed to be due to the Fe ions in ZnO that act as a quencher and the quenching of luminescence is attributed to the photo excited electrons, which are preferentially transferred to the iron ion induced trap centers in ZnO lattice **[15]**. However, the 1 mol% and 3 mol% of Fe doped ZnO exhibit only one peak around ~ 386 nm associated with near band (NB) ultra violet emission and is slightly shifted towards lower wavelength side, which corresponds to the NBE emission and hence there is no detectable signal of the well-known stronger and broader emission situated in the yellow-green part of the visible spectrum as shown in **Fig. 9.** Moreover, in the visible region of the PL spectra, there appears a broad emission band for 5 mol% of Fe doped ZnO superstructure in the range of 450-650 nm, with a peak around 574 nm. In particular, for 5 mol% of Fe doped ZnO, the NBE shifts slightly towards lower wavelength side (385 nm) and the green band is shifted to higher wavelength side (574 nm) in addition to the increase of intensity compared to pristine ZnO. The green band emission can be ascribed to singly ionized oxygen vacancies in ZnO **[32, 41, 42]**. However, the broad emission peaks become less intense and nearly quench the green-yellow luminescence for the 1 mol% and 3 mol% of Fe-doped ZnO samples, which shows a clear indication of the presence of Fe^{2+} in the ZnO nanocrystals. Therefore, the intensity of the UV emission is maximum for 1 mol% of Fe content and as the Fe content is increased (> 1 mol %) up to 5 mol%, the UV emission decreases, but not less than the intensity in the pristine ZnO. Here, the green emission peak intensity of 5 mol% of Fe doped ZnO samples is stronger than those in the other samples. The change in intensity, the shift in near band edge (NBE) emission from 388 to 385 nm and a shift in green band (GB) emission from 500 to 574 nm confirm the substitution

of Fe into the Zn–O lattice. The red shift of green emission peak is probably related to the Fe - related defect levels.

Magnetic properties

Fig. 10 (A) depicts the clear hysteresis loops of magnetization curve (M-H) of undoped and co-doped ZnO nanostructured plates and which are distinctive of soft magnetic materials at room temperature (300 K) in the field range of ± 10000 Oe. The present investigation of the all samples shows the ferromagnetic behavior. The $Zn_{1-(x+y)}Fe_xAg_yO$ (x= 0 mol%, 1 mol%, 3 mol%, and 5 mol%; y= 0 mol% and 5 mol%) samples at room temperature (300 K) exhibit the coercive field (H_c) and the remnant magnetization (M_r) of approximately 40.19, 70.13, 23.09 and 105.19 Oe and 0.0103, 0.0208, 0.0055 and 0.0267 emu/g respectively. In the present studies, coercive field (H_c) and remnant magnetization (M_r) values have increased with increase of Fe dopant in ZnO samples (except for ~ 3 mol% of Fe doped ZnO). The similar decrease of coercivity value for ~ 3.05 % of Fe doped ZnO nanorods have been reported by Limaye et al. **[15]**.

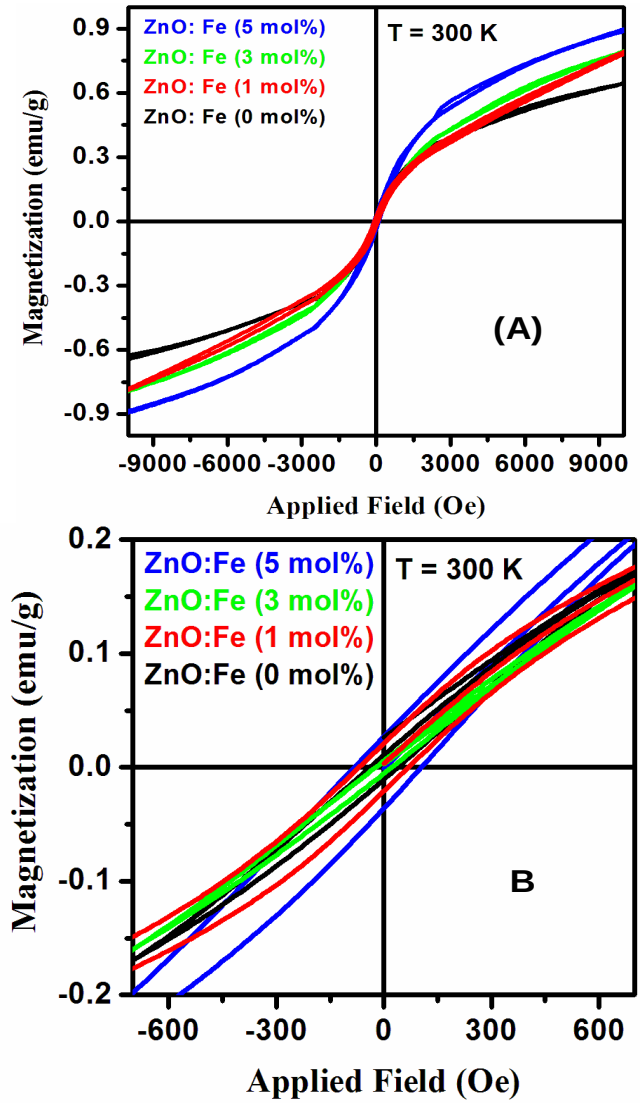

Fig. 10. (A) Depicts the magnetization curve (M-H) of undoped and (Fe, Ag) co-doped ZnO nanostrutured materials. (B) Shows the enlarged low field region of the hysteresis loops.

Further, **Fig. 10 (B)** shows the enlarged low field region of the hysteresis loops and definite coercivity of about 105.19 Oe is obtained. In the present study, the relative saturation magnetization (M_s) values of the four samples are found to show increase with increasing Fe doping content from x = 0 mol% to 5 mol%, as compared with the previous reports **[14, 43]**. It is observed that the value of saturation magnetization (M_s) increases from 0.305 emu/g for pristine ZnO to 0.451 emu/g for 5 mol% (Fe, Ag) doped ZnO nanoplates. Generally, there are three possible reasons for ferromagnetism. The first is defect related mechanism, which is often reported for DMSs **[14].** The second is secondary phases of impurities and the third one is micro Fe or Ag clusters. However, in the present study, there is no evidence of secondary phase in the XRD and HRTEM of co-doped ZnO nanoplates. Also signals of Ag or Fe clusters are not observed, which reveal that the Fe and Ag atoms successfully substitute the regular Zn sites. In the single phase XRD patterns, most intense peak (101) of the ZnO position suggests a small shift toward lower 2θ values with increasing of Fe doping and the evidence of Fe incorporation into ZnO from Raman and PL studies. The Raman peak intensity decreases with increasing of Fe in ZnO lattice, which indicates that more defects arise leading to ferromagnetism in the co-doped ZnO samples. It is strongly supported by PL studies. From all these observations, it can reasonably be concluded that the increase of ferromagnetism at laboratory temperature with the increase of iron dopant in ZnO, is due to defect related mechanism.

Conclusion

A large scale production of pristine and co-doped (Fe, Ag) ZnO nanostructured materials (plates) of average size ~ 100 and 50 nm have been obtained at various percentages of Fe through chemical precipitation method. The co-substitution of Fe and Ag does not disturb the wurtzite crystal structure of parent ZnO. On incorporation of Fe into ZnO, the fundamental phonon mode is A_1 (LO) obviously broadened and shifted by about 8 cm^{-1} towards lower energy, which reveal that the defects are considerable so as to make the co-doped ZnO material as ferromagnetic. From PL spectra, a shift in near band edge (NBE) emission and a shift in green band (GB) emission strongly suggest the substitution of Fe into the Zn–O lattice. Room temperature ferromagnetism (RTFM) gradually increases from 0.305 emu/g to 0.451 emu/g, with increasing of Fe content in ZnO lattice. Thus, the overall results show that the co-doped (Fe, Ag) ZnO nanostructures are suitable for the development of optoelectronic and spintronics devices.

Reference

1. Ohno, H.; Matsukura, F.; Ohno, Y. *JSAP Int.* **2002**, 5, 4. **DOI:** org/10.12785/jsap
Tiwari, A.; Mishra, A.K.; Kobayashi, H.; Turner, A.P.F. (Eds), In Intelligent Nanomaterials, WILEY-Scrivener Publishing LLC, USA, **2012**.
2. Zeng, H.B.; Cai, W.P.; Liu, P.S.; Xu, X.X.; Zhou, H.J.; Klingshrin, C.; Kalt, H. *ACS Nano.* **2008**, 2, 1661. **DOI:** 10.1021/nn800353q
Gulia, S.; Kakkar, R. *Advanced Materials Letters*, **2013**, 4, 876. **DOI:** 10.5185/amlett.2013.3440

3. Zeng, H.B.; Xu, X.J.; Bando, Y.; Gautam, U.K.; Zhai, T.Y.; Fang, X.S.; Liu, B.D.; Golberg, D. *Adv. Funct. Mater*. **2009,** 19, 3165. **DOI:** 10.1002/adfm.200900714
4. Huang, M.H.; Mao, S.; Feick, H.; Yan, H.Q.; Wu, Y.Y.; Kind, H.; Weber, E.; Russo, R.; Yang, P.D. *Science.* **2001,** 292, 1897. **DOI:** 10.1126/science.1060367
   Sanjay, S. S.; Yadav, R.S.; Pandey, A.C. *Advanced Materials Letters*, **2013**, 4, 378. **DOI:** 10.5185/amlett.2012.9427
5. **S**rivastava, P.; Sharma, Y. *Adv. Mat. Lett.* **2011**, 2(4), 290. **DOI:** 10.5185/amlett.indias.206
   Shukla, S. K.; Deshpande, S. R.; Shukla, S. K.; Tiwari, A. *Talanta*, **2012**, 99, 283.
6. Schwartz, D.A.; Gamelin, D.R. *Adv. Mater*. **2004,** 16, 2115. **DOI:** 10.1002/adma.200400456
7. Zhou, H.J.; Fallert, J.; Sartor, J.; Dietz, R.J.B.; Klingshirn, C.; Kalt, H.; Weissenberger, D.; Gerthsen, D.; Zeng, H.B.; Cai, W.P. *Appl. Phys. Lett*. **2008,** 92, 132112-1. **DOI:** org/+10.1063/1.2907197
8. Xiang, B.; Wang, P.W.; Zhang, X.Z.; Dayeh, S.A.; Alpin, D.Pr.; Soci, C.; Yu, D.P.; Wang, D.L. *Nano Lett*. **2007**, 7, 323. **DOI**: 10.1021/nl062410c
9. Yuan, G.D.; Zhang, W.J.; Jie, S.; Fan, X.; Zapien, J.A.; Leung, Y.H.; Luo, B.; Wang, P.F.; Lee, C.S.; Lee, S. T. *Nano Lett*. **2008,** 8, 2591. **DOI:** 10.1021/nl073022t
10. Gautam, U.K.; Panchakarla, L.S.; Dierre, B.; Fang, X.; Bando, Y.; Sekiguchi, T.; Govindaraj, A.; Golberg, D.; Rao, C.N.R. *Adv. Funct. Mater*. **2009**, 19, 131. **DOI**: 10.1002/adfm.200801259
11. Dietl, T.; Ohno, H.; Matsukura, F.; Cibert, J.; Ferrand, D. *Science*. **2000,** 287, 1019. **DOI**: 10.1126/science.287.5455.1019
12. Sato, K.; Katayama-Yoshida, H. *Jpn. J. Appl. Phys.* **2001**, 40, L334. **DOI:** 10.1143/JJAP.40.L334
13. Fukumura, T.; Jin, Z.; Ohtomo, A.; Koinuma, H.; Kawasaki, M. *Appl. Phys. Lett*. **1999**, 75, 3366. **DOI:** 10.1063/1.125353
14. Phanigrahy, B.; Aslam, M.; Bahadur, D. Nanotechnology, **2012**, 23, 115601-1. **DOI:** 10.1088/0957-4484/23/11/115601
15. Limaye, M.V.; Singh, S.B.; Das, R.; Poddar, P.; Kulkarni, S.K. *J. Solid State Chem.* **2011**,184, 391. **DOI:** 10.1016/j.jssc.2010.11.008
16. Glaspell, G.; Dutta, P.; Manivannan, A. *J. Cluster Sci*. **2005**, 16, 523. **DOI:** 10.1007/s10876-005-0024-y
17. Iqbal, J.; Wang, B.; Liu, X.; Yu, D.; He, B.; Yu, R. *New J. Phys*. **2009**, 11, 063009-1. **DOI:**10.1088/1367-2630/11/6/063009
18. Sharma, V.K.; Varma, G.D. *Adv. Mat. Lett.* **2012,** 3(2), 126. **DOI:** 10.5185/amlett.2011.7283
19. Rao, C.N.R.; Deepak, F.L. *J. Mater. Chem*. **2005**, 15, 573. **DOI:** 10.1039/B412993H
20. Alaria, J.; Bieber, H.; Colis, S.; Schmerber, G.; Dinia, A. *Appl. Phys. Lett*. **2006,** 88, 112503. **DOI:** 10.1063/1.2186079
21. Kolesnik, S.; Dabrowski, B. *J. Appl. Phys.* **2004,** 96**,** 5379. **DOI:** 10.1063/1.1755428
22. Garcia, M.A.; Merino, J.M.; Fernandez Pinel, E.; Quesada, A.; De La Venta, J.; Ruiz Gonzalez, M.L.; Castro, G.R.; Crespo, P.; Liopis, J.; Gonzalez-Calbet, J.M.; Hernando, A. *Nano lett.* **2007**, 7, 1489. **DOI:** 10.1021/nl070198m
23. Li, H.; Huang, Y.; Zhang, Q.; Qiao, Y.; Gu, Y.; Liu, J.; Zhang, Y. *Nanoscale*, **2011**, 3, 654. **DOI:** 10.1039/c0nr00644k
24. X. Qiu, L. Li, C. Tang and G. Li, *J. Am. Chem. Soc.*, **2007,** 129, 11908. **DOI:** 10.1021/ja074630d
25. Sankara Reddy, B.; Venkatramana Reddy, S.; Venkateswara Reddy, P.; Koteeswara Reddy, N. *Opt. Adv. Mat. – Rap. Comm.* **2012,** 6, 953. **URL:** http://oam-rc.inoe.ro/index.php?option=magazine&op...
26. Shah, A.H.; Basher Ahamed, M.; Manikandan, E.; Chandramohan, R.; Iydroose, *M. J. Mater. Sci. Mater. Electron.* **2013.** **DOI:** 10.1007/S10854-013-1093-6
    Shukla, S.K.; Tiwari, A.; Parashar, G.K.; Mishra, A.P.; Dubey, G.C. *Talanta*, **2009**, 80, 565.
27. He, M.; Tian, Y.F.; Springer, D.; Putra, I.A.; Xing, G.Z.; Chia, E.E.M.; Cheong, S.A.; Wu, T. *Appl. Phys. Lett*. **2011**, 99, 222511-1. **DOI:** 10.1063/1.3665401
28. Chen, A.J.; Wu, X.M.; Sha, Z.D.; Zhuge, L.J.; Meng, Y.D. *J. Phys. D: Appl. Phys*. **2006**, 39 4762. **DOI:** 10.1088/0022-3727/39/22/004
29. Singhal, A.; Achary, S.N.; Tyagi, A.K.; Manna, P.K.; Yusuf, S.M. *Mater. Sci. Eng. B*. **2008,** 153, 47. **DOI:** 10.1016/j.mseb.2008.09.030
30. Wang, C.; Chen, Z.; He, Y.; Li, L.; Zhang, D. *Appl. Surf. Sci.* **2009,** 255, 6881. **DOI:** 10.1016/j.apsusc.2009.03.008
31. Liu, C.; Meng, D.; Pang, H.; Wu, X.; Xie, J.; Yu, X.; Chen, L.; Liu, X. *J. Magn. Magn. Mater.* **2012,** 324, 3356. **DOI:** org/10.1016/j.jmmm.2012.05.054
32. Ekambaram, S.; Iikubo, Y.; Kudo, A. *J. Alloys Compd.* **2007**, 433, 237. **DOI:** org/10.1016/j.jallcom.2006.06.045
33. Dinesha, M.L.; Prasanna, G.D.; Naveen, C.S.; Jayanna, H.S. *Indian J Phys.* **2013**, 87(2), 147. **DOI:** 10.1007/s12648-012-0182-3
34. Alim, K.A.; Fonoberov, V.A.; Shamsa, M.; Balandir, A.A. *J. Appl. Phys*. **2005**, 97, 124313. **DOI:** 10.1063/1.1944222
35. Schumm, M. ZnO based semiconductors studied by Raman spectroscopy: semimagnetic alloying, doping and nanostructures, Ph.D. thesis, Julius Maximilians-Universitat Wurzburg, 2008. **Urn:** nbn: de: bvb:20:opus-37045
36. Liu, J.M.; Ong, C.K.; Lim, L.C. *Ferroelectrics.* **1999**, 231, 223. **DOI:** 10.1080/00150199908014535
37. Youn, C.J.; Jeong, T.S.; Han, M.S.; Kim, J.M. *J. Cryst. Growth*. **2004,** 261, 526. **DOI:** 10.1016/j.jcrysgro.2003.09.044
38. Pandiyarajan, T.; Udayabhaskar, R.; Karthikeyan, B. *Spectrochim Acta A*. **2013,** 103, 173. **DOI:** 10.1016/j.saa.2012.10.028
39. Erhart, P.; Albe, K.; Klein, A. *Phys. Rev. B*. **2006,** 73, 205203-1. **DOI:** 10.1103/PhysRevB.73.205203
40. Borse, P.H.; Deshmukh, N.; Shinde, R.F.; Date, S. K.; Kulkarni, S.K. *J. Mater Sci.* **1999**, 34, 6087. **DOI:** 10.1023/A:1004709601889
41. Qiu, Y.; Yang, S. *Adv. Funct. Mater*. **2007**, 17, 1345. **DOI:** 10.1002/adfm.200601128
42. Yang, Z.X.; Zhong, W.; Au, C.T.; Du, X.; Song, H.A.; Qi, X.S.; Ye, X.J.; Xu, M.H.; Du, Y.W. *J. Phys. Chem. C*. **2009**, 113, 21269. **DOI:** 10.1021/jp903130t
43. Saleh, R.; Prakoso, S.P.; Fishli, A. *J. Magn. Magn. Mater*. **2012**, 324, 665. **DOI:** 10.1016/j.jmmm.2011.07.059